Journal of Molecular Liquids 363 (2022) 119802

Contents lists available at ScienceDirect

Journal of Molecular Liquids

journal homepage: www.elsevier.com/locate/molliq

Design and synthesis of multifunctional polymeric micelles for targeted delivery in *Helicobacter pylori* infection

Aimen Qaiser [a], Maria Hassan Kiani [b], Rashida Parveen [c], Muhammad Sarfraz [d], Gul Shahnaz [a,*], Abbas Rahdar [e,*], Pablo Taboada [f,*]

[a] Department of Pharmacy, Faculty of Biological Sciences, Quaid-i-Azam University, Islamabad 45320, Pakistan
[b] Department of Pharmacy, Iqra University, Islamabad, Pakistan
[c] Department of Pharmacy, Superior University Lahore, Pakistan
[d] College of Pharmacy, Al Ain University, Al Ain 64141, United Arab Emirates
[e] Department of Physics, University of Zabol, Zabol 98613-35856, Iran
[f] Grupo de Física de Coloides y Polímeros, Departamento de Física de Partículas e Instituto de Materiales (IMATUS), Universidade de Santiago de Compostela, 15782 Santiago de Compostela, Spain

ARTICLE INFO

Article history:
Received 10 May 2022
Revised 4 July 2022
Accepted 5 July 2022
Available online 9 July 2022

Keywords:
Nanomicelles
Targeted delivery
Mucoadhesion
Mucopenetration
H. pylori infection

ABSTRACT

This study aimed to design a hyaluronic acid-based targeted, mucoadhesive and mucopenetrating drug delivery system encapsulating clarithromycin that would improve the drug residence time at *H. pylori* infection site. Clarithromycin-loaded thiolated hyaluronic acid-co-oleic acid (CLR-thHA-co-OA), clarithromycin-loaded ureido-conjugated thiolated hyaluronic acid-co-oleic acid (CLR-Ur-thHA-co-OA), and clarithromycin-loaded papain-modified ureido-conjugated thiolated hyaluronic acid-co- oleic acid (CLR-PAP-Ur-thHA-co-OA) nanomicelles were prepared by an ultra-sonication method. FTIR data confirmed the successful grafting of the different ligands to polymer backbone. XRD analysis revealed the amorphous nature of the polymer conjugate and drug inside nanomicelles. The critical micelle concentration of PAP-Ur-thHA-co-OA nanomicelles was found to be 15.85 μg/ml. Also, the sizes of nanomicelles were in the range of 210–258 nm. TEM analysis of CLR-PAP-Ur-thHA-co-OA nanomicelles confirmed their small size and spherical shape. Zeta potential and entrapment efficiency of CLR-PAP-Ur-thHA-co-OA nanomicelles were –24 mV and 80 ± 7.2% respectively. A sustained drug release pattern was observed for all types of prepared nanomicelles, whereas CLR-PAP-Ur-thHA-co-OA ones also displayed improved stability at acidic pH. Due to the presence of thiol groups in the polymer backbone, thiolated nanomicelles displayed important mucoadhesive properties. In this regard, FDA loaded PAP-Ur-thHA-co-OA nanomicelles showed the deepest penetration distance into the mucus by cleavage of mucoglycoproteins when compared to papain-unmodified nanomicelles. Fluorescent images of gastric tissues revealed the greater gastric retention time of nanomicelles compared to the free drug. As consequence, an enhanced *in vitro* efficacy against *H. pylori* was observed by nanomicelles. The *in vivo* clearance study showed an improved eradication of *H. pylori* by CLR-PAP-Ur-thHA-co-OA nanomicelles in comparison to other nanoformulations. Thus, the newly synthesized CLR-PAP-Ur-thHA-co-OA nanomicelles have the potential to be used as an efficient nanocarrier for *H. pylori* infection treatment due to their enhanced mucopenetration and mucoadhesion properties, as well as their improved stability and extended drug release.

1. Introduction

Helicobacter pylori (H. pylori), a gram-negative, non-invasive, microaerophilic, a spiral bacterium is known as a major pathogen associated with peptic ulcer [1], duodenal ulcer [2], gastritis [3], mucosa-associated lymphoid tissue (MALT) lymphoma [4] and gastric carcinoma [2,5], and has been classified as class I carcinogen by the World Health Organization (WHO). According to estimations, *H. pylori* colonizes more than 50% of the world's inhabitants, infecting the majority in their childhood [6]. This bacterium resides in the deeper layer of gastric mucosa or at the surface of the epithelial cells throughout the life of an individual. The presence of *H. pylori* is usually harmless, but it can cause peptic ulcer disease or other chronic diseases in 5–10%

* Corresponding authors.
E-mail addresses: gshahnaz@qau.edu.pk (G. Shahnaz), a.rahdar@uoz.ac.ir (A. Rahdar), pablo.taboada@usc.es (P. Taboada).

https://doi.org/10.1016/j.molliq.2022.119802
0167-7322/

population [7]. Various treatment strategies like standard triple therapy including two antibiotics and a proton pump inhibitor for 7–14 days or a quadruple therapy containing bismuth in addition to the recommended triple therapy for 10 days have been used in clinics [8,9]. However, these therapeutic options are currently inefficacious to eradicate the microbe due to most common antibiotic resistance, inability of antibiotics to cross the mucosal barrier, antibiotic deterioration at acidic pH, therapeutic non-compliance, and inadequate residence time in the gastric region [10,11].

To circumvent these hurdles, different strategies have been investigated including mucoadhesive, and/or muco-penetrating and/or pH-sensitive drug delivery nanocarriers [10,12]. Nanocarriers have gained much attention as promising oral drug delivery systems for the treatment of *H. pylori* infection due to their several advantageous properties such as mucoadhesivity, biocompatibility and biodegradability. Hyaluronic acid has been widely used in different pharmaceutical dosage forms i.e., ocular inserts, buccal patches, tablets, hydrogels and scaffolds [13–15]. It is a biocompatible and biodegradable anionic polymer with promising mucoadhesive properties [16]. Owing to such properties, it can be used in many oral liquid dosage forms to improve their residence time and subsequent efficacy of pharmaceutical products. Therefore, hyaluronic acid has been investigated for its use in drug delivery systems as a cornerstone for effective drug delivery. Moreover, this biopolymer can be chemically modified as it contains hydroxyl and carboxylic groups that can react with a variety of molecules resulting in multifunctional drug delivery system [17]. In particular, thiomers have been considered to improve mucoadhesion properties as well as imparting mucopenetrating properties of drug delivery nanosystems; and their combination with mucolytic enzymes like papain incorporated to a nanocarrier system should provide new ways to reach the pathogen infection site in deep mucus layer. This nanocarrier system may be generated by further modifying the hyaluronic acid backbone with oleic acid to create a block copolymer able to self-assemble into polymeric nanomicelles. Polymeric nanomicelles are self-assembling nano-constructs of amphiphilic copolymers having a core–shell shape. The hydrophobic core encapsulates hydrophobic components that are protected from the external physiological environment by a hydrophilic corona [18]. However, there has not been much research about using hyaluronic acid-based polymeric nanomicelles in drug delivery for the eradication of *H. pylori* infection.

Therefore, our study aimed at developing of papain-modified ureido-conjugated thiolated hyaluronic acid-co-oleic acid (PAP-Ur-thHA-co-OA) nanomicelles for the effective eradication of *H. pylori*. Initially, hyaluronic acid was thiolated by carbodiimide chemistry to improve its mucoadhesive characteristics. Thiolated hyaluronic acid was then hydrophobically modified by oleic acid to prepare polymeric nanomicelles by ultrasonication. Oleic acid, an unsaturated fatty acid, has been suggested to possess bacteriostatic and bactericidal properties against a wide range of bacteria [19]. Urea, specifically recognized by Urel protein on *H. pylori* membrane, was then grafted to the polymer backbone being used as a targeting moiety to the infection site [20]. Mucopenetrating properties were imparted to the nanocarrier system through the attachment of the mucolytic enzyme, papain. The designed PAP-Ur-thHA-co-OA nanomicelles incorporating clarithromycin as a model drug were evaluated for their mucoadhesive, mucopenetrating, release characteristics and *in vitro* efficacy against *H. pylori*. The developed nanomicelles are proposed to have improved mucoadhesion, mucopenetration and efficacy against the pathogen residing in the deep mucus layer.

2. Experimental

2.1. Materials

Clarithromycin was obtained from Global Pharmaceuticals (Pakistan). Hyaluronic acid (HA), N-hydroxysuccimide (NHS), urea, oleic acid were from Sigma Aldrich, Germany. Cystamine hydrochloride was purchased from Daejung China. Ellman's reagent (Di thio-bis nitro benzoic acid was from Alfa Aesar (Germany), whereas papain was obtained from Merck (Germany). EDAC (Ethyl dimethyl aminopropyl carbodiimide, Penicon), casein powder (Science Home, Pakistan), Fluorescein diacetate (FDA) was from Avonchem (United Kingdom). Hydrochloric acid was bought at Riedel-De-haen, RDH, Labor chemikalein, GmBh & Co (Germany). Potassium dihydrogen phosphate, sodium dihydrogen phosphate, dipotassium hydrogen phosphate, sodium hydroxide, acetone, and sodium chloride were from Scharlau (Germany. Distilled water was from MilliQ grade (Department of Pharmacy, QAU, Islamabad).

Bacterial strain of *Helicobacter pylori* was obtained from Microbiology Department of Quaid-i-Azam University, Islamabad. Swiss albino mice were purchased from National Institute of Health (NIH), Islamabad.

2.2. Methodology

2.2.1. Synthesis of thiolated hyaluronic acid (thHA)

Thiolated hyaluronic acid was synthesized through an EDAC coupling reaction [21]. In brief, sodium hyaluronate (0.2 g) was dissolved in 50 mL distilled water. The pH was then adjusted to 5.5 using 0.1 N HCl. Then, 50 mM N-hydroxy succinimide and 1-ethyl-3-(3-dimethylaminopropyl) carbodiimide hydrochloride were added to the above solution and stirred for 15 min. The pH of the mixture was adjusted to 5.5. Cystamine hydrochloride (0.25 g) was added to the mixture followed by pH adjustment to 6.0. Stirring was done for 4 h at 25 °C in dark. Dialysis against 1% NaCl three times and one time against distilled water were carried out in dialysis tubes to get rid of unreacted material. The polymer was lyophilized at −50 °C after dialysis and kept at 4 °C.

2.2.2. Synthesis of thiolated hyaluronic acid-co-oleic acid (thHA-co-OA) conjugate

Hyaluronic acid-co-oleic acid (thHA-co-OA) conjugate was also synthesized through an EDAC coupling reaction [22]. Briefly, a solution of thiolated hyaluronic acid was made by adding 1 g of thiolated hyaluronic acid in 60 mL of water and 5 M HCl (pH < 5). Next, 0.57 g of oleic acid was dissolved in 40 mL ethanol followed by the addition of 100 mM EDAC and stirred at 60 °C for 30 min. The activated OA solution was poured into the hyaluronic acid one under vigorous stirring and the reaction was carried out at 80 °C for 24 h. The resulting mixture was then dialyzed (dialysis membrane M_w cut off 3.5 kDa) for 3 days against deionized water in the absence of light at 10 °C and freeze dried at −45 °C. The resulting conjugate was stored at 4 °C until further use.

2.2.3. Synthesis of ureido modified thHA-co-OA conjugate

Ureido-modified hyaluronic acid-co-oleic acid (Ur-thHA-co-OA) conjugate was synthesized by carbodiimide reaction [23] with few modifications. In short, 1 g of thHA-co-OA conjugate was dissolved in 500 mL of water following the addition of 20 mL of EDAC/NHS solution (502 mg EDAC and 302 mg NHS). The mixture was allowed to react for 5 min. Then, urea solution was made by dissolving 72 mg of urea in 1 mL DMSO. This solution was poured into the polymeric one and left to react for 12 h at 25 °C. The final solution was dialyzed (dialysis membrane M_w cut off 3.5 KDa) for

4 days against excess of water and 0.3 M NaCl solution. The dialyzed sample was lyophilized and stored at 4 °C until further use.

2.2.4. Synthesis of papain modified ureido conjugated hyaluronic acid-co-oleic acid conjugate (Pap-Ur-thHA-co-OA)

Papain-modified ureido-conjugated thiolated hyaluronic acid-co-oleic acid (Pap-Ur-thHA-co-OA) conjugate was synthesized also by carbodiimide reaction [21]. Briefly, 1% (w/v) solution of Ur-thHA-co-OA conjugate was prepared by solubilizing 1 g of conjugate in 100 mL of water. pH of the solution was adjusted to 6 with 5 M NaOH solution. 500 mg of EDAC and 300 mg of NHS were then added to the polymer solution and the mixture was stirred for 2 h. Thereafter, papain solution was prepared by solubilizing 100 mg of papain in 50 mL of water and added to the polymer solution slowly while stirring. This mixture was stirred at 10 °C for 12 h. Dialysis was carried out for 48 h in dark at 10 °C against deionized water. The dialyzed mixture was then freeze dried and stored at 4 °C.

2.3. Characterization of the polymer

2.3.1. Degree of conjugation

The number of thiol groups attached to the polymeric backbone was determined spectrophotometrically by using the Ellmańs reaction as previously described [24]. Briefly, 0.5 mg of hyaluronic acid-cystamine (thHA) conjugate was dissolved in 250 μL of deionized water followed by the addition of 250 μL of phosphate buffer (5 M, pH 8.0). Then, 0.5 mL of Ellman's reagent prepared by dissolving 3 mg of Ellman's reagent in 10 mL of phosphate buffer 5 M, pH 8.0, was added. The sample was incubated for 2 h in dark and centrifuged. The supernatant was separated and added into a 96 well plate to measure its absorbance at 450 nm using a microplate reader (Perkin Elmer, USA). The thiol groups grafted to the polymer chain were quantified using the standard curve of L-cysteine hydrochloride.

2.3.2. Disulfide bond formation

The degree of disulfide bond formation was determined by means of the Ellman's test [25,26]. Briefly, 0.5 mg of polymer was dissolved in 350 μL of deionized water. 650 μL of phosphate buffer (0.5 M, pH 6.8) was added to this mixture under continuous stirring for 30 min at 37 °C. Then, 1 mL of a 4% (w/v) solution of sodium borohydride was added to this mixture and incubated for 1 h at 37 °C. Thereafter, 5 M HCl (200 μL) solution was added to the former solution mixture to remove unreacted KH_2PO_4, and then reacted with 0.2 mL of Ellman's reagent (15 mg solubilized in 5 mL of phosphate buffer, pH 6.8) and stirred. Aliquots of 300 μL were added to a 96-well plate microplate after 1 h and evaluated at 450 nm using a microtiter plate reader (Perkin Elmer, USA). The concentration of attached cysteine was determined by previously established calibration curve. The degree of disulfide bonds formation was measured by subtracting he absorbance of free thiol groups from that of total thiol groups.

2.3.3. Determination of Critical micelle concentration (CMC)

The Critical Micelle Concentration (CMC) of the resulting copolymer was determined by a dye solubilization method. Pyrene was used as the dye probe and the CMC determined by fluorescent spectrophotometry (Perkin Elmer LS50, USA) [27]. A solution of pyrene in methanol was prepared by solubilizing 3 mg pyrene in 50 mL methanol. A volume of this pyrene solution (50 μL) was added to different polymer (PAP-Ur-thHA-co-OA) solutions with changing concentrations from 0.001 to 1000 μg/mL and incubated overnight to achieve equilibrium. The excitation spectra of pyrene were scanned in the range of 250–360 nm at a constant emission wavelength of 390 nm. At the CMC, a sharp rise in the intensity ratio (I338/I333) of pyrene was observed. The ratio was calculated and plotted against log values of nanomicelle concentration. CMC value was obtained at the intersection point of two straight lines at low and high polymer concentration regimes.

2.3.4. Evaluation of swelling behavior

The swelling behavior of polymeric conjugates/copolymers i.e., thHA-co-OA, Ur-thHA-co-OA and PAP-Ur-thHA-co-OA was evaluated using a gravimetric method [28]. Polymeric discs/tablets of the different conjugates were prepared by compression (single punch machine, Emmy, Pakistan) of lyophilized powders of respective conjugates into 5.0 mm flat faced tablets of 30 mg each while keeping a constant compaction pressure. Tablets were then immersed in phosphate buffer (pH 6.8) at 37 °C after being attached to a syringe needle. The discs were removed from the medium and weighed accurately at specific time intervals. The quantity of buffer absorbed was calculated as a function of time by using the equation:

$$\textit{Swelling ratio}\ (\%) = \frac{W_t - W_0}{W_0} \times 100 \quad (1)$$

Here, W_0 denotes the weight of the disc in the dry state and W_t the weight of the wet swollen disc at time t, respectively.

2.3.5. Preparation of polymeric nanomicelles

Various process parameters for the synthesis of Pap-Ur-thHA-co-OA nanomicelles were optimized by applying central composite design (CCD) by using Design Expert software v7.0. Optimization of the independent variables i.e., Pap-Ur-thHA-co-OA concentration, and percentage of drug (w/w of polymer concentration) was done by the response surface methodology (RSM). The percentage entrapment efficiency (EE) and particle size of nanomicelles were used as response parameters. Nanoformulations were formulated as per the runs generated by the software. The results obtained were entered the software and evaluated for statistical significance. p value < 0.05 indicated a significant model. The appropriate model for each response was chosen based on adequate precision, noise ratio, probability, adjusted R^2 value and predicted R^2 value. Polymer concentration was varied from 0.59 mg/mL to 3.14 mg/mL and the weight percentage of drug added, (w/w) of polymer concentration, was between 25.86% and 54.14%.

Briefly, clarithromycin was dissolved in acetone using different percentages of drug according to the weight of the polymer conjugate. Different concentrations of Pap-Ur-thHA-co-OA polymer as reported by design expert were hydrated in 5 mL water and clarithromycin solutions were added to the polymer solutions followed by stirring at 65 °C for 30 min to evaporate acetone [29]. The mixtures were then sonicated using a probe sonicator for 20 min at 25 °C (Fig. 1). Afterwards, the solutions were centrifuged for 20 min at 10,000 rpm to get rid of unloaded drug. Clarithromycin-loaded nanomicelles were washed with water and freeze dried.

2.3.6. Fluorescein diacetate (FDA) labeling of polymeric nanomicelles

Fluorescein diacetate (FDA) was incorporated into thHA-co-OA, Ur-thHA-co-OA and PAP-Ur-thHA-co-OA nanomicelles for penetration study [30]. Drug and polymer/polymer conjugates solutions were made and added to 0.1% (w/v) solution of FDA in acetone. The nano micelle suspensions were then stirred for 2 h in dark at 15 °C. The FDA-labeled nanomicelles were then centrifuged to remove excess of FDA, re-dispersed in water and freeze-dried.

2.4. Characterization of nanomicelles

2.4.1. Physical characteristics of nanomicelles

Physico-chemical characteristics of nanomicelles including particle size, zeta potential, and polydispersity index (PDI) were

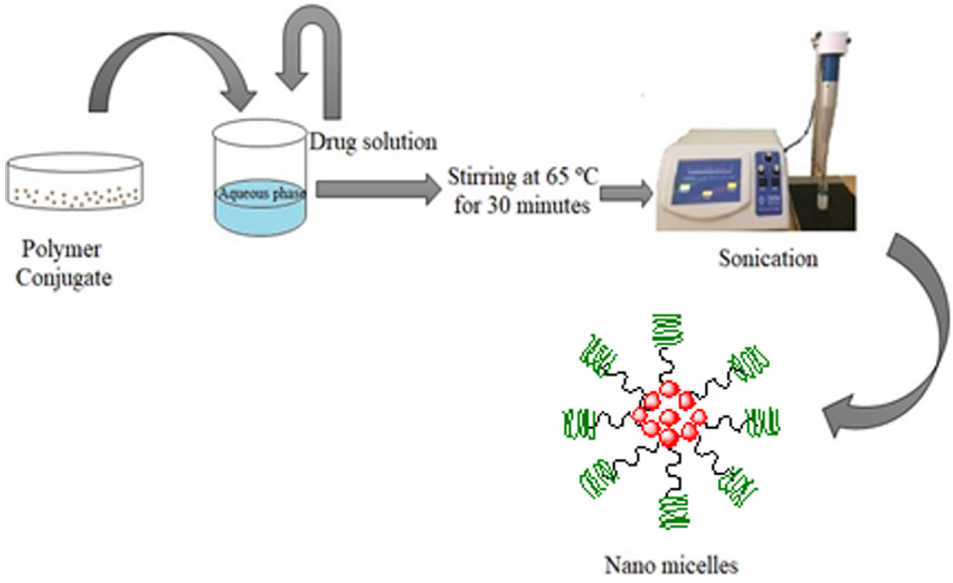

Fig. 1. Preparation of drug-loaded polymeric nanomicelles.

determined using dynamic light scattering and Doppler anemometry using a Nanozeta sizer (Malvern, UK). Samples were diluted with distilled water and stirred at room temperature before analysis to avoid changes in electrophoretic mobility of nanomicelles due to aggregation. The size and morphology of the formed nanomicelles were also confirmed by transmission electron microscopy (TEM). For that, a droplet of the tested formulation was placed on a carbon coated copper grid and dried at room temperature. Filter paper was used to eliminate the remaining traces of liquid dispersion. A drop of 2% (v/v) phosphotungstic acid solution was added, and the excess solution was discarded with filter paper once again. The sample was air-dried before being examined using a TEM microscope (LEO912-AB, Zeiss, Germany).

2.4.2. Fourier transform Infrared (FTIR) spectroscopy

Fourier Transform Infrared (FTIR) spectra of drug, enzyme, oleic acid, polymer, and polymer conjugates, urea and nanomicelles were acquired using a FTIR spectrophotometer (Bruker alph-P, USA) equipped with an ATR (attenuated total reflectance) accessory. Before acquiring spectra, a blank background scan was performed keeping the cell plate empty. For tests, small amounts of powdered sample were placed at the pike miracle of the ATR cell completely covering the surface of the of ZnSe crystal to form a compact mass. Samples were scanned over a range of 4000 cm^{-1} to 600 cm^{-1} with a resolution of 2 cm^{-1}, collected, and peaks assigned.

2.4.3. Powder X-ray diffraction analysis

Powder X-ray diffractometer (Bruker, D2 Phaser USA) was used to determine the crystalline nature of pure drug-polymer conjugates and nanomicelles. The device was adjusted at an angle between 20° and 70° and a step size of 0.5505 was used.

2.4.4. Entrapment efficiency (EE%)

The EE% was calculated by separating the nanomicelles from the aqueous medium by ultracentrifugation [31]. The unbound drug in the supernatant was assessed spectrophotometrically. The entrapment efficiency was measured by the difference of current drug amount added in nanocarrier and free drug in supernatant. Entrapment efficiency was calculated using the equation:

$$\text{Entrapment efficiency } \% = \frac{\textit{Total amount of drug} - \textit{Amount of unbound drug}}{\textit{Total Amount of drug}} \times 100 \quad (2)$$

2.4.5. In vitro drug release

A dialysis tube method was used to determine the *in vitro* release of the drug (CLR) from free drug suspension, CLR-thHA-co-OA, CLR-Ur-thHA-co-OA and CLR-PAP-Ur-thHA-co-OA and CLR-PAP-Ur-thHA-co-OA nanomicelles at pH 6.8 for 48 h at 37 ± 0.5 °C. Drug release from CLR-PAP-Ur-thHA-co-OA nanomicelles was also assessed at pH 1.2 for 24 h at 37 ± 0.5 °C. 5 mL of sample were taken inside dialysis tube in 1000 mL of deionized water to maintain sink conditions. At predefined time points, samples were withdrawn, and drug content was measured by UV–Vis spectroscopy (Shimadzu, UV-1800, Japan) at 210 nm. The mechanism of drug release from nanomicelles was determined by applying different kinetic models (zero order, first order, Higuchi, Korsmeyer Peppas and Hixon-Crowel).

2.4.6. Evaluation of mucoadhesive properties through rheological study

A cone-plate viscometer was used to determine the rheological properties of nanomicelles [32]. Briefly, a dispersion of artificial mucin was made by adding 5 g artificial mucin in 100 mL of 6.8 pH phosphate buffer. Then, each nanomicelle suspension (1 mL) was mixed with the mucin dispersion (5 mL) and the mixtures were then incubated at 37 ± 0.5 °C. The viscoelastic properties of each nanomicelle suspension were determined at 1 h, 2 h, 4 h and 6 h at 50 s^{-1} shear rate.

$$\Delta\eta = \eta_{mix} - \eta_{muc} \quad (3)$$

where η_{mix} is the apparent viscosity of the mixture of nanomicelles and mucin (Pa.s) and η_{muc} is the viscosity of the mucin dispersion (standard).

2.4.7. In vitro penetration study

A silicon tube method with little modification was used to determine the mucopenetrating properties of polymeric nanomicelles [32]. Mucus was separated and purified as described in a

method reported previously [33]. Firstly, a small portion of goat upper small intestine was excised and collected from slaughtered house, and immediately transferred to an icebox. The intestine was washed thoroughly with normal saline to remove the debris material. Afterwards, the intestine was everted to open the mucosal side, and rinsed with normal saline. Mucus was collected in a jar by scraping off with a sharp object. The collected mucus was purified with NaCl (0.1 M) and stored at – 20 °C until further use. 34 mm long silicon tubes of 0.2 mm internal diameter were filled with purified mucus (400 μL) and were sealed at one end. Then, each FDA-labelled micelle formulations (60 μL) dispersed in 6.8 pH phosphate buffer was poured into the silicon tubes through the other end and sealed. 400 μL of pure mucus served as blank. All the silicon tubes were incubated for 4 h at 37 °C with horizontal shaking and then kept at −25 °C for at least 12 h. The frozen tubes were sliced into 16 pieces of 2 mm. To each slice, 500 μL of 5 M NaOH were added followed by incubation at 37 °C to hydrolyze FDA to colored sodium fluorescein. The samples were then sonicated for 30 min and analyzed spectrophotometrically at 490 nm to measure the soluble sodium fluorescein and calculate hence the percent penetration of micelles into each slice.

2.4.8. Gastric retention of nanomicelles

Male albino mice of 25 g weight were divided into 3 groups randomly (n = 6) to be treated with rhodamine labelled PAP-Ur-thHA-OA nanomicelles for 4 and 24 h [34]. Control group was not treated with dye labelled nanomicelles. 0.5 mL of rhodamine labelled PAP-Ur-thHA-OA nanomicelles were administered orally to each mouse through oral gavage in the remaining two groups. Mice were killed at 4 h and 24 h after treatment and stomach tissues were excised. Stomach tissues were washed with PBS to remove excess nanomicelles and tissue grafts were prepared for fluorescent imaging.

2.4.9. In vitro antibacterial assay

An *in vitro* antibacterial assay was carried out using an approach previously outlined [35]. *H. pylori* clinical isolates were chosen for this study, and biopsy samples were obtained. The biopsy material was immediately homogenized in brucella broth. *H. pylori* strains were grown in a microaerophilic environment (5% O_2, 10% CO_2, and 85% nitrogen) at 37 ± 0.5 °C. *H. pylori* were cultivated on chocolate agar medium for 5 days. The growth of *H. pylori* was measured using optical density (OD) as a measuring parameter utilizing spectrophotometric analysis at a wavelength of 600 nm. In 1 mL of broth, 1 OD is said to equal 108 colony forming units. Identification procedures, including morphological evaluation, were performed on the microorganisms. After that, test tubes comprising of 5 mL of nutrient broth and a full loop of strain were prepared for the *in-vitro* growth inhibition test. After that, nanomicelles and pure free clarithromycin suspension at double the minimum inhibitory concentration (MIC) value of antibiotic were added to the foregoing mixtures. As a control, a tube containing pure culture was used. The tubes were incubated at 37 ± 0.5 °C with constant shaking and a microaerophilic atmosphere. 50 μL sample obtained from these tubes at various time points were put on Skirrow's medium in Petri dishes and incubated for 4 h at 37 ± 0.5 °C in microaerophilic conditions. Thereafter, the colonies present on all agar plates were quantified. The % inhibition was determined by the given equation:

$$\text{Percent inhibition}(\%) = \frac{\textit{Number of colonies of given mixture}}{\textit{Number of colonies of pure strain}} \times 100 \quad (4)$$

2.4.10. In vivo clearance investigation of H. Pylori

In vivo clearance of *H. pylori* was investigated using the previously reported Qian's method [36]. *H. pylori* was extracted from gastritis patients. To do that, 0.3 mL broth comprising 10^9 colony forming units (CFU) of *H. pylori* were inoculated in stomach of 6 weeks old male Wistar rats. After 4 weeks of injection the infection was confirmed through morphology and rapid urease test. Free clarithromycin, clarithromycin-loaded thiolated hyaluronic acid-co-oleic acid (CLR-thHA-co-OA), clarithromycin-loaded ureido-conjugated thiolated hyaluronic acid-co-oleic acid (CLR-Ur-thHA-co-OA) and clarithromycin-loaded papain-modified ureido-conjugated thiolated hyaluronic acid-co- oleic acid (CLR-PAP-Ur-thHA-co-OA) nanomicelles were administered orally at a dose of 5, 7.5 and 10 mg/kg. Physiological saline was used as a control. After one day of administration, the rats were killed to remove their stomach. Stomaches were sliced and tissues were smeared in modified skirrow's medium followed by incubation for 3 days at 37 °C in microaerophilic conditions. Viable bacterial cells were calculated by counting the bacterial colonies that appeared on agar plates. Colonies were also studied for morphology and rapid urease test.

3. Results and discussion

3.1. Synthesis and characterization of polymer

Helicobacter pylori (*H. pylori*) is the most prevailing and ubiquitous pathogen, inhabiting half of the world's population. Poor stability of conventional treatment regimens, their short retention time and bacterial resistance have led to treatment failures. The development of nanoscale drug delivery systems is becoming very attractive to address different shortcomings and issues related to conventional therapies for *H. pylori*. Gastrointestinal mucosa is a thick viscous layer composed of glycoproteins offering a biological barrier [37]. The properties of this barrier and high mucus turnover rate clear out nanocargoes from mucosa prior to penetration of the nanocarrier to the deep mucosal layer colonized with *H. pylori* [38]. Thiolated nanocarriers have been developed as a promising strategy to increase the residence time of nanoformulations in the gastrointestinal tract (GIT), resulting in improved bioavailability and therapeutic efficacy since they exhibit strong mucoadhesive characteristics by means of disulfide bond formation with cysteine regions of GI mucosa. Along with mucoadhesive characteristics, thiolated nanocarriers should also hold mucopenetrating properties to facilitate the access to pathogen hiding in the deep mucosal layer [39]. In addition, the specific active targeting of nanocarriers to *H. pylori* infection sites can be achieved by means of the nanosystem surface modification with different ligands or molecules. *H. pylori* contains *Urel* protein for the transport of urea into the cell in order to produce an alkaline environment for bacteria survival; for this reason, an ureido modification of the developed nanocarriers may be a good strategy to achieve a site-specific targeting and therapeutic action [20].

In this study, hyaluronic acid was used owing to its mucoadhesive and antibacterial properties [40]. Thiolated hyaluronic acid (thHA) was synthesized by carbodiimide reaction, see Fig. 2**(a).** The thiol groups attached to the polymer backbone tend to improve the mucopenetration and mucoadhesive characteristics of hyaluronic acid [25]. Unsaturated fatty acids have been reported to have antibacterial activity [41]. Thus, conjugation of oleic acid to hyaluronic acid imparts improved antibacterial activity to the resulting conjugated polymer. Oleic acid was conjugated to thiolated hyaluronic acid *via* carbodiimide reaction **(**Fig. 2**(b))** forming a thHA-co-OA conjugate that imparted hydrophobic characteristics to the polymer conjugate, resulting in an amphiphilic polymer that can self-assemble into nanomicelles in aqueous solutions [42]. Conjugation of urea to the thHA-co-OA polymer conjugate was done by a coupling reaction through amide bond formation, see

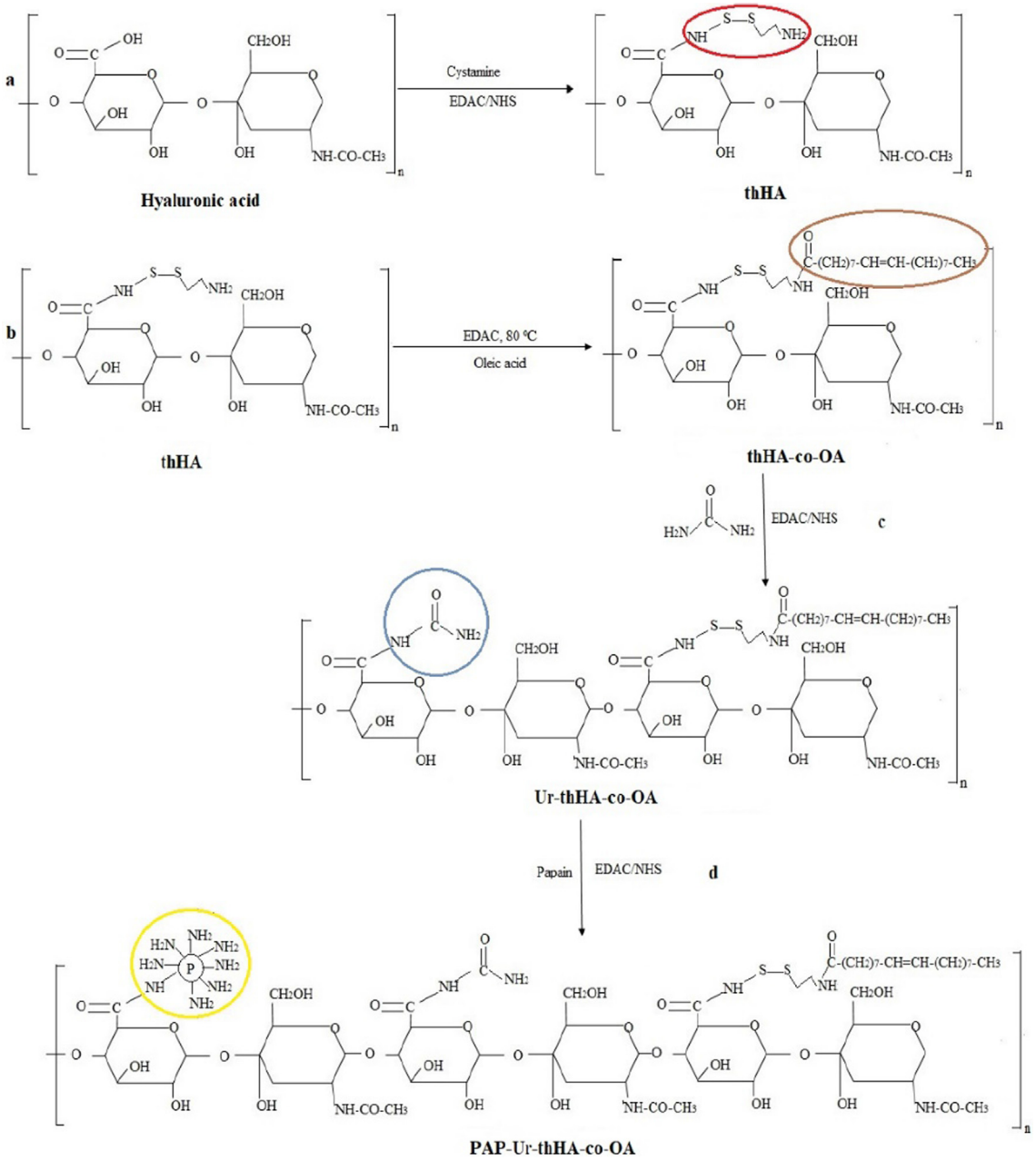

Fig. 2. Scheme of polymer conjugates preparation. Step (a) synthesis of thiolated hyaluronic acid (thHA) conjugate, (b) formation of thiolated hyaluronic acid and oleic acid (thHA-co-OA) conjugate, (c) synthesis of ureido-conjugated thiolated hyaluronic acid - oleic acid (Ur-thHA-co-OA) conjugate, and (d) synthesis of papain-modified ureido-conjugated oleic acid grafted thiolated hyaluronic acid conjugate (PAP-Ur-thHA-co-OA).

Fig. 2**(c).** Conjugation of urea imparted site-specific characteristics to polymer conjugate directing the nanocarrier system to *Urel* protein located on the membrane of *H. pylori* [43], as mentioned before. In addition, a papain-modified ureido-conjugated thiolated hyaluronic acid-co-oleic acid (PAP-Ur-thHA-co-OA) conjugate was also synthesized through the formation of amide bond between the carboxylic acid groups of hyaluronic acid and amino groups of papain, see Fig. 2**(d).** Papain then was covalently attached to polymer backbone. The conjugated enzyme has manifested an improved stability and less susceptibility to denaturation than the free enzyme [44].

The attachment of cystamine, oleic acid, urea and papain on hyaluronic acid was confirmed by FTIR analysis, see Fig. 3**.** Pure hyaluronic acid showed the common carbonyl stretching peak at 1720 cm^{-1} and a stretching band at 3443 cm^{-1} confirming carboxylic and hydroxyl groups within the polymer structure, respectively [45]. The stretching peak at 2366 cm^{-1} in the thHA conjugate confirms the presence of cystamine SH groups onto the polymer chains [46]. Amide bond formation in thHA was confirmed by the presence of amide band at 1557 cm^{-1}. Oleic acid spectrum showed the C=O stretching band at 1710 cm^{-1} and C=C stretching at 1500 cm^{-1} [47]. In the case of pure urea, stretching peaks at 1457 cm^{-1}, 1673 cm^{-1} and 3425 cm^{-1} corresponding to C—N, C=O and NH stretchs, respectively, were observed [48]. The peak at 1631 cm^{-1} in thHA-co-OA conjugate confirmed the presence of amide bond in the polymer structure. In the case of Ur- thHA-co-OA conjugate, the presence of amide bond is confirmed by the presence of stretching peaks at 1645 cm^{-1} and 1554 cm^{-1}. The FTIR spectrum of free papain showed peaks at 1632 cm^{-1} and 3276 cm^{-1} indicating C=O and NH stretchs of

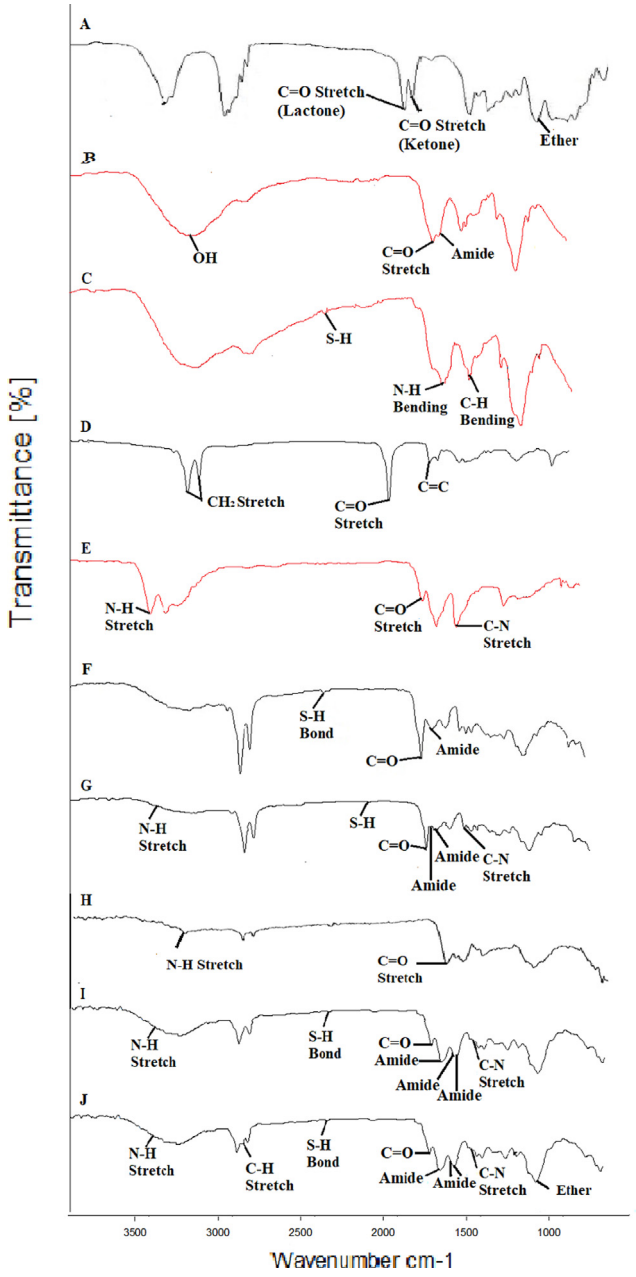

Fig. 3. FTIR spectra of clarithromycin (A), hyaluronic acid (B), thiolated hyaluronic acid (C), oleic acid (D), urea (E), thHA-co-OA conjugate (F), Ur-thHA-co-OA conjugate, (G), papain (H), PAP- Ur-thHA-co-OA conjugate (I) and CLR-Ur-thHA-co-OA nanomicelles.

papain. Papain-modified polymer conjugate showed additional peaks at 1637 cm^{-1} and 1570 cm^{-1} indicating the formation of amide bond and, thus, the successful conjugation of papain to polymer conjugate.

In addition, the swelling behavior of thHA-co-OA, Ur-thHA-co-OA and PAP-Ur-thHA-co-OA polymers was evaluated by immersion of thin flat discs made of such polymeric conjugates in phosphate buffer (pH 6.8). Swelling analysis was performed to illustrate the impact of thiolation and papain modification on the swelling properties of the polymer, see Fig. 4**a**. This is important since swelling influences mucoadhesion, drug release profile and stability [49]. The diffusion between polymer and mucus layer is favored by enhanced water absorption, which results in strong mucoadhesion [50]; hence, a moderate swelling of the polymer is beneficial for an effective mucoadhesion process [51]. The disc made of PAP-Ur-thHA-co-OA displayed an abrupt water uptake and swelling during the first 15 min of incubation, and then the increase is more gradual and the water uptake was retained constant for ca. 90 min, which is necessary for suitable mucoadhesion. At this respect, it is worth mentioning that the pH of thiolated hyaluronic acid plays a major role in the improvement of swelling behavior [52]. The pH of thHA-co-OA conjugate was <5. By increasing the pH above 3, H^+ ion concentration decreases, and the amount of cysteine groups immobilize on the polymer increases resulting in improved mucoadhesive properties of the polymer. Papain-modified polymer showed an increased swelling as compared to bare thiolated polymer due to the presence of hydrophilic groups in addition to thiol moieties [53], thus, expecting to favor mucoadhesion, and thus, prolonged drug release, retention and stability.

3.2. Synthesis and characterization of nanomicelles

Critical Micelle Concentration (CMC) of polymer conjugates (PAP-Ur-thHA-co-OA) determined by pyrene assay was found to be 15.9 μg/ml, see Fig. 4**b.** The low CMC value indicated the great amphiphilic character of the polymeric conjugates giving rise to stable micelles able to be suitable for drug delivery [27].

Optimization of nanomicelle formulations was carried out by employing Design Expert Software v7.0 to choose the most appropriate values of independent parameters by central composite design (CCD). Based on the impact of response variables, a point at optimal area was chosen where % entrapment efficiency was maximum and particle size was minimum. Then optimized parameters were predicted on the basis of desirability factor (0.779). These were A: 1.89 mg/ml (polymer concentration), B: 33.11% of drug with predicted values of 260.338 nm and 79.49%, for particle size and % entrapment efficiency respectively. Significant effects of independent variables on response variables (particle size and entrapment efficiency) were observed. An increase in entrapment efficiency was observed as the polymer concentration and drug percentage do probably as positive consequence of hydrophobic interactions between the cargo and the polymer, creating a suitable environment inside the nanomicelle core [54]. A similar positive impact was found in determining particles size by increasing the concentration of independent variables. A significant increase in particle size with the polymer concentration was observed [55]. The selected optimized formulation was again formulated and contrasted with the predicted results shown in Table 1. These data indicated that experimental analysis and anticipated values were nearly similar supporting the probability of CCD model at nano level.

Clarithromycin-loaded thHA-co-OA and Ur-thHA-co-OA nanomicelles were prepared by using different initial drug percentages according to initial polymer weight by means of a sonication method. The nanoformulations with small size and PDI <0.5 were selected and further characterized. Similarly, CLR-loaded PAP-Ur-thHA-co-OA nanomicelles were successfully prepared by the same sonication method using the optimized values of independent variables derived from Design Expert software. The nanomicelles were formed at a polymer concentration of 1.89 mg/ml with 33.11% drug.

The IR spectrum of clarithromycin showed the C═O stretch of lactone ring at 1728 cm^{-1} and the C═O stretch of ketone at 1689 cm^{-1} and the peak at 1167 cm^{-1} is related to the ether group (not shown) [56]. The successful loading of the drug into the nanomicelles was confirmed by the presence of specific peaks of clarithromycin and papain in the FTIR spectrum of the final nanoformulation (CLR-PAP-Ur-thHA-co-OA, Fig. 3), not observing interaction between the polymer conjugate and drug.

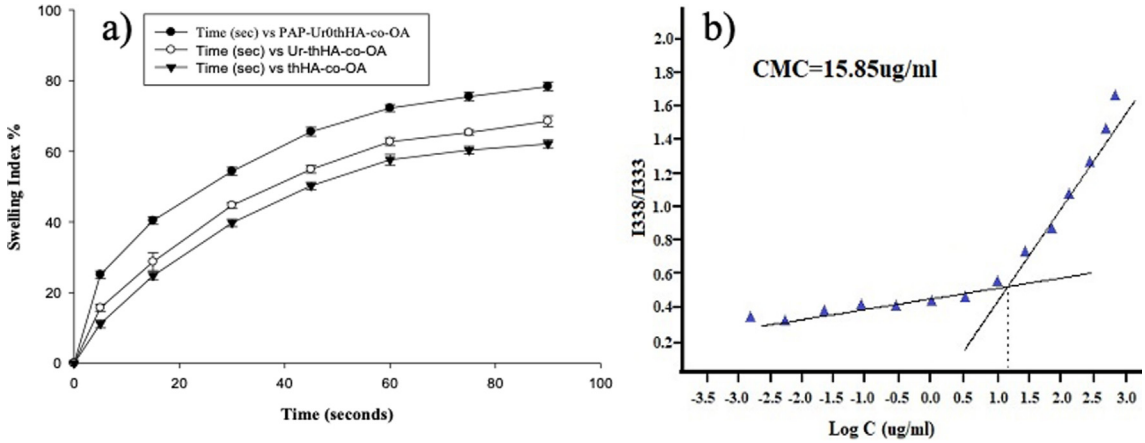

Fig. 4. (a) Swelling of thHA-co-OA, Ur-thHA-co-OA and PAP-Ur-thHA-co-OA conjugates in phosphate buffer (pH 6.8, 0.1 M): (b) Critical Micelle Concentration of PAP-Ur-thHA-co-OA polymer conjugate.

Table 1
Observed and anticipated response values for optimized nanomicelles formulation.

Response	Anticipated values	Observed values
EE (%)	79.5	80.1
Particle size (nm)	260	258

EE: Entrapment efficiency.

Characteristic peaks of clarithromycin were observed in the XRD pattern of the free drug form that were screened in the XRD data of the final nanoformulation, i.e., CLR-PAP-Ur-thHA-co-OA, see Fig. 5**a**. These data demonstrated that during formulation design, the crystalline nature of the drug may be lost and transform into a more amorphous form. Likewise, the XRD of nanomicelles also showed a decrease in the height of the characteristic peaks

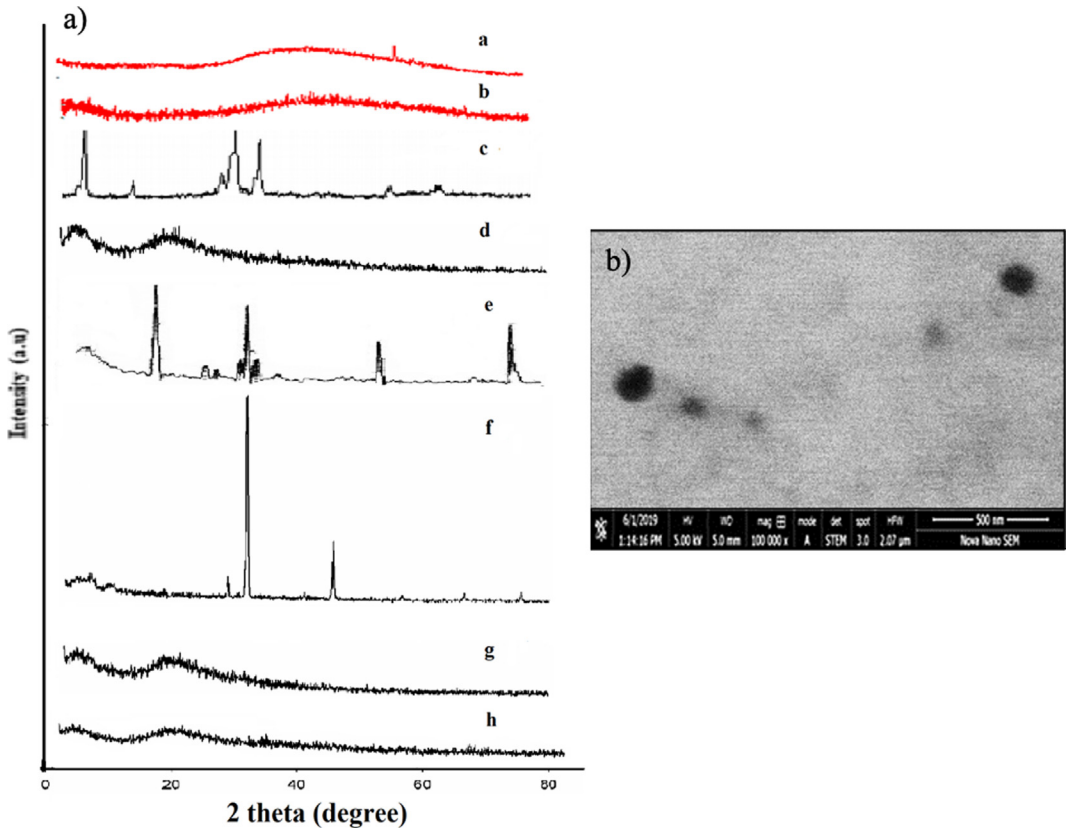

Fig. 5. *(a)* X-ray diffraction spectra of pure drug, polymer conjugates and nanomicelles. (a) Hyaluronic acid, (b) thiolated hyaluronic acid, (c) clarithromycin, (d) thiolated hyaluronic acid-co-oleic acid conjugate, (e) urea, (f) ureido-conjugated thiolated hyaluronic acid-co-oleic acid conjugate, (g) Papain-modified ureido-conjugated thiolated hyaluronic acid-co-oleic acid conjugate, and (h) clarithromycin-loaded papain-modified ureido-conjugated thiolated hyaluronic acid-co-oleic acid nanomicelles. *(b)* TEM image of PAP-Ur-thHA-co-OA nanomicelles.

of polymer, urea and polymer conjugates providing evidence that the crystalline structure of the polymer may also transform into a more amorphous state during the development of nanoformulation.

Particle size, entrapment efficiency, polydispersity index and zeta potential of allnano formulations are shown in Table 2**.** Particle size of these nanomicelles was in the range of 210–258 nm having a negative zeta potential which accounts with the presence of carboxylic groups of hyaluronic acid. The shape and size of final nano formulation was analyzed by TEM analysis. As shown in Fig. 5**b** the nanomicelles displayed spherical shape and particle size <300 nm. Zeta potential values greater than +25 mV or less than −25 mV of nano formulations represent highly stable nanosuspensions thanks to inter-particle repulsive forces [57]; alternatively, low zeta potential values can lead to particle aggregation due to Wan der Waals attractive interactions between particles resulting in physical instability of nanosuspensions [58]. In this regard, thiolated hyaluronic acid-co-oleic acid nanomicelles showed a smaller particle size with highly negative zeta potential; conversely, urea and papain modifications of nanomicelles caused an increase in the particle size. Highly negative zeta potentials of ca. –33.0 mV were observed for 210 nm-sized nanomicelles of CLR-thHA-co-OA, while CLR-PAP-Ur-thHA-co-OA nanomicelles with particle size of 258 nm exhibited a zeta potential of −24.4 mV indicating stable nanoformulation; that is, the negative values of zeta potential decreased with urea and papain conjugation, and smaller particles have high zeta potential values for improved stability as compared to large sized particles [59]. In addition, all the nanomicelles had PDI value<0.45 confirming uniform size population distribution, whereas the entrapment efficiency (EE%) of nanomicelles was not affected with urea and papain modifications. The size distribution analysis of various nanomicelles has been presented in Fig. 6.

3.3. In vitro release profile

The *in vitro* clarithromycin release profile from free CLR suspension, CLR-thHA-co-OA, CLR-Ur-thHA-co-OA and CLR-PAP-Ur-thHA-co-OA nanomicelles was assessed for a period of 48 h at pH 6.8 (Fig. 7**a**), and CLR release from CLR-PAP-Ur-thHA-co-OA nanomicelles was assessed at 1.2 pH (Fig. 7**b**) for 24 h under sink conditions by dialysis. The percentage of clarithromycin released from the different formulations was time-dependent, with a biphasic drug release pattern composed of an initial burst release phase of the drug followed by a more sustained and prolonged release behavior. The initial burst release that occurred within the first few hours of incubation may be due to a relatively small amount of drug present at the interface between the micelle hydrophobic core and hydrophilic corona [60].

CLR-PAP-Ur-thHA-co-OA, CLR-thHA-co-OA and CLR-Ur-thHA-co-OA nanomicelles exhibited a cumulative release of 85%, 76% and 79% after 48 h at 6.8 pH, respectively. For thiolated nanomicelles, drug release is controlled by gradual swelling and breakage of disulfide linkages within polymer matrix. In the case of CLR-PAP-Ur-thHA-co-OA nanomicelles, these include a mucolytic enzyme in addition to thiol groups that involves a reduction in disulfide bonding within polymer structure, thus, increasing the swelling properties and favoring an enhanced cumulative drug release after 48 h. Conversely, only 11% of drug was released at

Table 2
Physicochemical characterization of Clarithromycin loaded of thHA-co-OA, Ur-thHA-co-OA and PAP-Ur-thHA-co-OA nanomicelles.

Nano formulations	Particle size (nm)	EE (%)	PDI	Zeta potential (mV)
thHA-co-OA	195	–	0.17	−28.1
CLR-thHA-co-OA	210	83 ± 12	0.19	−33.0
CLR-Ur-thHA-co-OA	226	81.2 ± 6	0.25	−32.2
CLR-PAP-Ur-thHA-co-OA	258	80 ± 9	0.25	−24.4

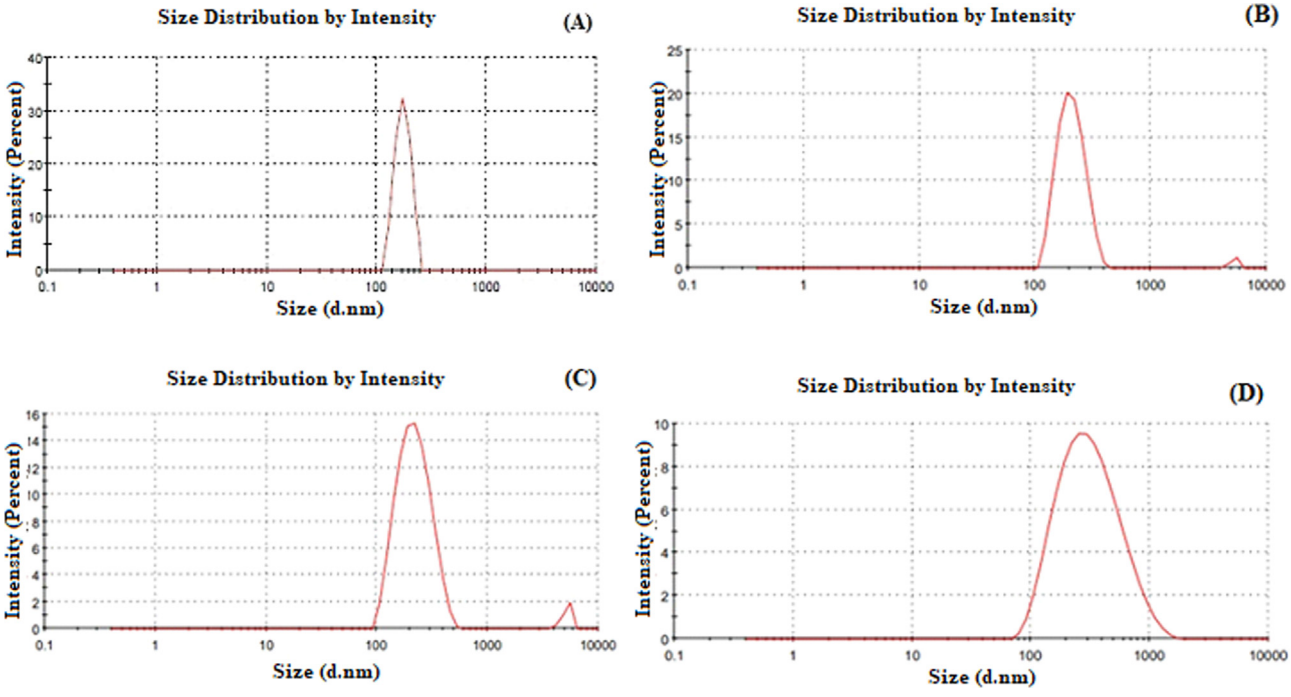

Fig. 6. Size distribution analysis of (A) thHA-co-OA, (B) CLR-thHA-co-OA, (C) CLR-Ur-thHA-co-OA and (D) CLR-PAP-Ur-thHA-co-OA polymeric micelles.

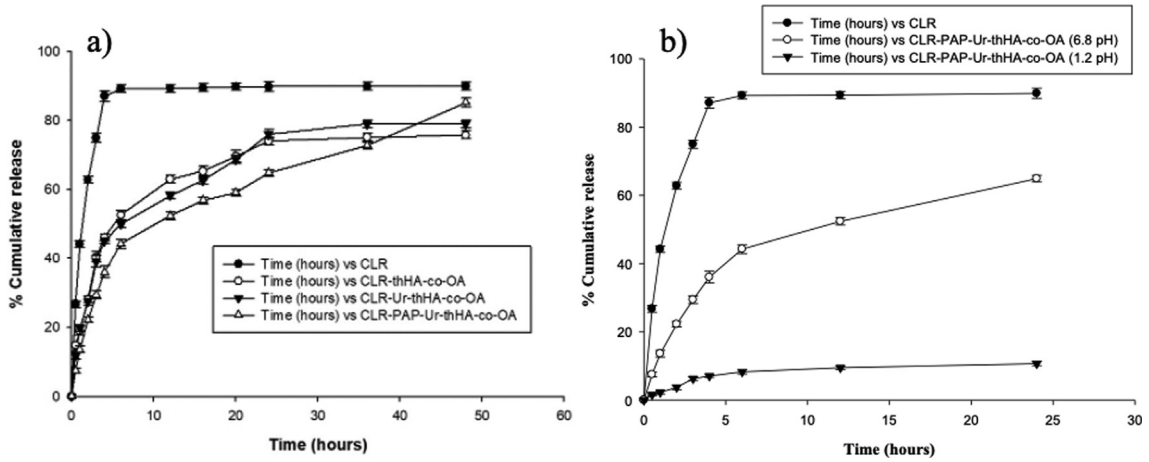

Fig. 7. (a) *In-vitro* CLR release from free CLR suspension, CLR-thHA-co-OA, CLR-Ur-thHA-co-OA and CLR-PAP-Ur-thHA-co-OA nanomicelles in phosphate buffer (pH 6.8) by dialysis for 48 h. (b) Comparison of clarithromycin release from CLR-PAP-Ur-thHA-co-OA nanomicelles in buffer of pH 1.2 and pH 6.8 by dialysis for 24 h. The values are noted as ± SD of means (n = 3).

Table 3
Drug release kinetics based on *in vitro* clarithromycin release from nanomicelles.

Formulation	Zero order	First order	Higuchi model	Korsmeyer-Peppas model		Hixon Crowell model
	$Q_t = Q_0 + K_0t$	$Q_t = Q_0e\text{-}Kt$	$Q = KH\ t_{1/2}$	$F = (M_t/M) = Km\ tn$		$W_t^{1/3} = W_0 - k^{1/3}\ t$
pH 6.8	**R^2**	**R^2**	**R^2**	**n**	**R^2**	**R^2**
CLR-thHA-co-OA	−0.1665	0.6858	0.7574	0.290	0.9479	0.5637
CLR-Ur-thHA-co-OA	0.0369	0.7554	0.8337	0.316	0.9639	0.6550
CLR-PAP-Ur-thHA-co-OA	0.4407	0.8380	0.9481	0.392	0.9810	0.7641
pH 1.2						
CLR-PAP-Ur-thHA-co-OA	0.1762	0.2330	0.8696	0.377	0.9214	0.2140

1.2 pH after 24 h from CLR-PAP-Ur-thHA-co-OA nanomicelles compared to ca. 65% at 6.8 pH, confirming the stability of nanomicelles at acidic pH. The thiol groups in the polymer structure are stable at pH < 5 [50]; thus, the polymeric structural composition protects the nanomicelles from degradation and prevent the release of drug at acidic pH.

Different kinetic models of drug release i.e. First order, Zero order, Higuchi, Korsmeyer Peppas and Hixson-Crowell, were used to model the drug release data obtained from CLR-thHA-co-OA, CLR-Ur-thHA-co-OA and CLR-PAP-Ur-thHA-co-OA nanomicelles. Table 3 shows the results of the kinetic analysis. Drug release data from all the nanomicelles i.e., CLR-thHA-co-OA, CLR-Ur-thHA-co-OA and CLR-PAP-Ur-thHA-co-OA ones seemed to follow the Korsmeyer-Peppas model, with n values < 0.45 in agreement with a Fickian diffusion controlled mechanism and prolonged drug release.

The stability of nanocarriers for oral drug delivery is influenced by the GIT environment and transit time. Nanomicelles prepared for oral drug delivery will first encounter the buccal cavity, in which they should experience a minimum degradation since the short residence time. In stomach drug loaded nanomicelles are exposed to an acidic environment. The polymeric coating of nanomicelles should protect the drug from degradation at gastric milieu and minimize drug release at acidic pH. These nanomicelles should then be directed towards the mucosal layer near the epithelial cells (pH 6–7) where *H. pylori* resides [20]. The residence time in stomach is large as compared to the buccal cavity, so that nanomicelles may penetrate in deep mucosal layer thanks to the mucolytic properties of the papain moiety grafted in the nanocarrier. In addition, nanomicelles owing to the presence of urea will target *H. pylori* residing in deep mucosal layer and release the drug causing bacterial eradication. The release analysis indicated the stability of the nanoformulation in *in vitro* environment mimicking the gastric milieu allowing the potential release of the drug at the infection site.

3.4. Rheology analysis

A cone-plate viscometer was used to determine the rheological characteristics of formed nanomicelles to assess their mucoadhesive behavior using artificial mucin. The obtained results are shown in Fig. 8. Interaction between mucin and nanomicelles causes a change

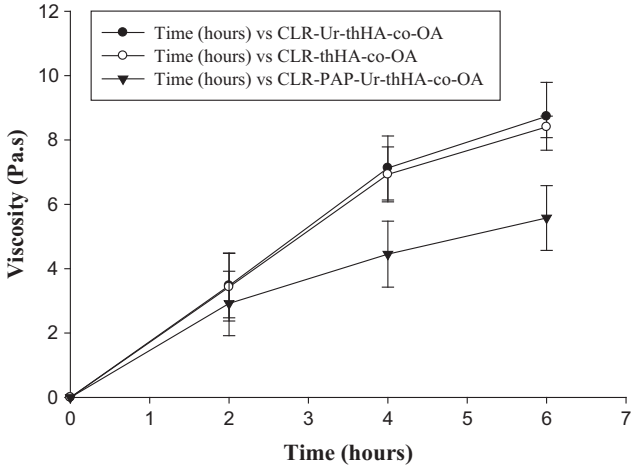

Fig. 8. Rheology analysis of thHA-co-OA, Ur-thHA-co-OA and PAP-Ur-thHA-co-OA nanomicelles.

in viscosity of both molecules that influences the mucoadhesion strength. Mucoadhesion is directly proportional to the changes in dynamic viscosity (Δη); the stronger the interaction between mucin or mucus, the higher will be the viscosity [61]. Thiolated polymers form disulfide linkages with cysteine rich regions of mucus and improved mucoadhesion, which may also be facilitated by some covalent or van der Waals interactions along with disulfide interchange reactions [62]. Thus, thiol groups present in thiolated nanomicelles form covalent bonds *via* disulfide linkages with the mucus layer, thus, enhancing the viscosity of the nanoformulation, improving the adhesion of nanocarriers to the mucus layer and, hence, exhibiting strong mucoadhesive characteristics. In this manner, CLR-thHA-co-OA nanomicelles showed ca. 1.56 times enhanced viscosity as compared to enzyme-modified nanocarriers. CLR-Ur-thHA-co-OA nanomicelles also showed an increase in viscosity after 6 h. CLR-PAP-Ur-thHA-co-OA nanomicelles displayed a reduced viscosity as compared to papain-unmodified nanocarriers in agreement with the incorporation of papain in addition to thiol moieties, that breaks linkages in mucoglycoproteins and accounting for the observed reduced viscoelastic properties. Hence, CLR-PAP-Ur-thHA-co-OA nanomicelles demonstrated both mucoadhesive and mucopenetrating characteristics.

3.5. Quantification of FDA in nanomicelles

FDA was loaded in nanomicelles for penetration studies. After incorporation, this molecule is retained in nanomicelles through lipophilic interaction. The FDA content was found to be 75% in FDA-thHA-co-OA, 70% in FDA-Ur-thHA-co-OA, and 66% in FDA-PAP-Ur-thHA-co-OA nanomicelles, respectively, confirming the successful loading inside nanomicelles.

3.6. Penetration study via silicon tube method

A silicon tube method with slight modification was used to make penetration studies on freshly separated mucus (see Fig. 9**a**). Deep mucosal penetration was observed up to the last 16 segment i.e., 34 mm distance, with papain-modified nanomicelles (PAP-Ur-thHA-co-OA). This result is originated thanks to the presence of the enzyme grafted within the nanocarrier system, which causes the lysis of mucoglycoproteins and leading to deep mucosal penetration. Ur-thHA-co-OA nanomicelles and thHA-co-OA nanomicelles showed lower detection values in last segments as compared to papain-modified ones. The PAP-Ur-thHA-co-OA nanomicelles exhibited both mucoadhesive and mucopenetrating characteristics as the hyaluronic acid based nanomicelles bear negative zeta potential due to the carboxylic acid groups in the polymer backbone. Because of these negative charges, the nanocarriers are repelled by sialic and sulfonic acid groups of mucus membrane and facilitate their transportation to the deeper parts. Furthermore, the human GIT mucus layer is composed of a linear peptide called mucin. This peptide forms a glycosidic linkage to different polysaccharides [63]. The mucus layer is highly protected from proteolytic activity and microbes because of these

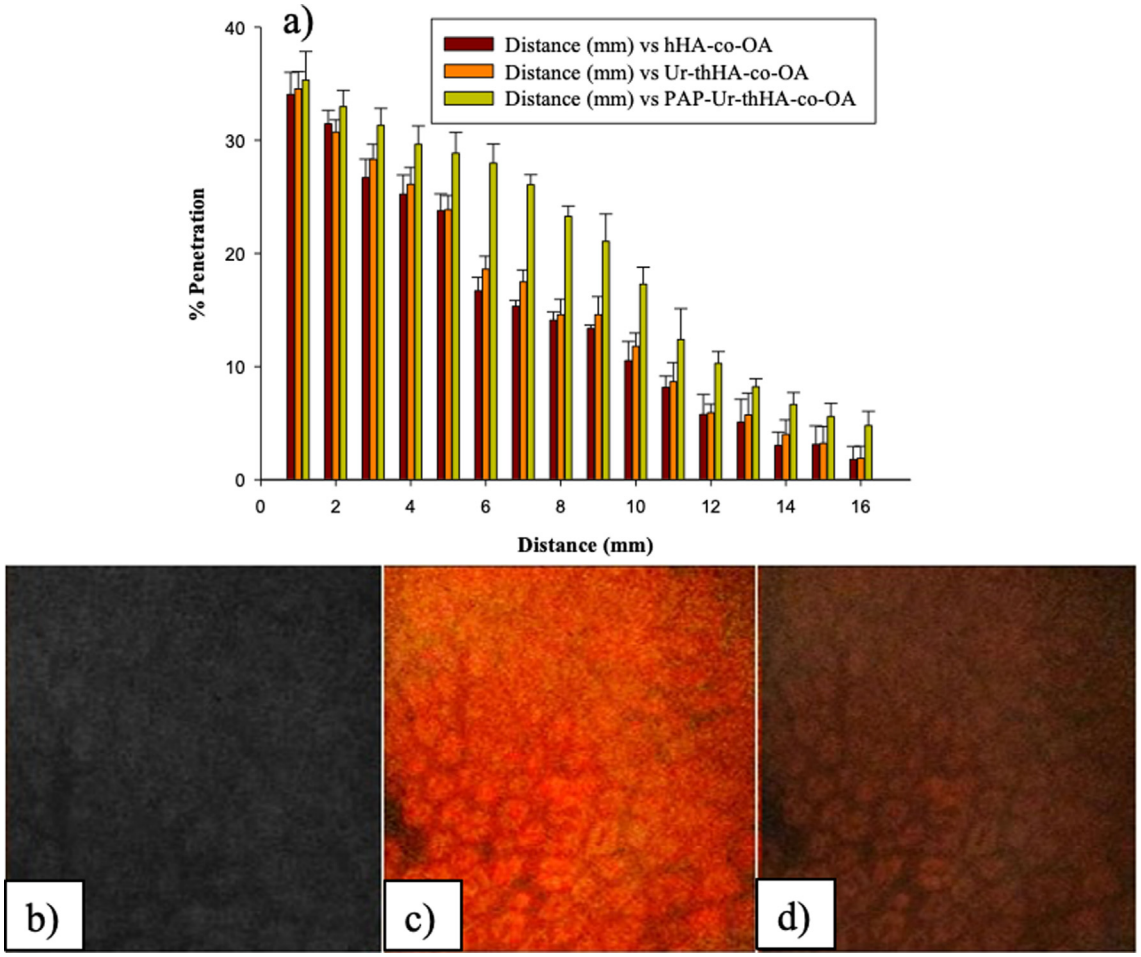

Fig. 9. (a) Penetration studies of FDA-labeled CLR-thHA-co-OA, CLR-Ur-thHA-co-OA and CLR-PAP-Ur-thHA-co-OA nanomicelles by a silicon tube approach at 37 °C. Retention analysis of PAP-Ur-thHA-co-OA nanomicelles in gastric cells of mice. (b) fluorescent image of untreated control group mouse gastric cells at 0 h. Fluorescent image of mouse gastric cells at (c) 4 h after and (d) 24 h of administration of rhodamine-labelled PAP-Ur-thHA-co-OA nanomicelles.

branched polysaccharides regions. In addition to polysaccharide chains which are hydrophilic, the mucus layer also possesses hydrophobic moieties. This region is uncovered and sensitive to enzymatic lysis. Papain specifically cleaves these peptide domains composed of 110 amino acids with several cysteine groups [37]. As a result of mucolytic activity, the woven matrix of mucin breaks down and penetration of nanomicelles is enhanced through the mucus. The unchanged glycoproteins in mucus can interact with nanomicelles through their cysteine rich regions; moreover, the continuous secretion of mucus causes improved mucoadhesion through disulfide exchange events. Improved penetration and adhesion of nanomicelles to deep mucosa hence increases the nanoformulation residence time in GIT that results prolonged interaction of nanomicelles with epithelial cells and prevents clearance of nanomicelles from mucosal layer by surrounding gastric medium [50].

3.7. Gastric retention of nanomicelles

Retention of rhodamine-labelled PAP-Ur-thHA-OA nanomicelles in mice stomach was studied by oral administration of such type of nanocarrier to mice. Next, stomachs of mice were removed after 4 and 24 h of nanomicelles administration. The stomach tissues were then subjected to fluorescence microscopy. The stomach tissues obtained at 4 h showed a strong fluorescence, which was longer than the reported gastric emptying time; meanwhile, those stomachs obtained at 24 h showed less intense fluorescence patterns (see Fig. 9**b–d**). As *H. pylori* resides in deep mucus layer on the surface of epithelial cells, the intended nanoformulation should be capable of reaching the deep mucosal layer and adhere to the mucus for effective *H. pylori* infection treatment.

3.8. In vitro antibacterial activity

The *in vitro* antibactericidal potential of CLR-thHA-co-OA, CLR-Ur-thHA-co-OA, CLR-PAP-Ur-thHA-co-OA nanomicelles and free clarithromycin suspension against *H. pylori* was evaluated by the colony count method. Free drug suspension and drug-loaded nanoformulations doubled the MIC value of drug. Antibacterial potential of drug suspension and nanoformulations increased with time (see Fig. 10). Free clarithromycin suspension showed a maximum eradication of 43.5% in 24 h. A gradual increase in growth inhibition was observed with nanomicelles: CLR-thHA-co-OA and, CLR-Ur-thHA-co-OA and CLR-PAP-Ur-thHA-co-OA showed

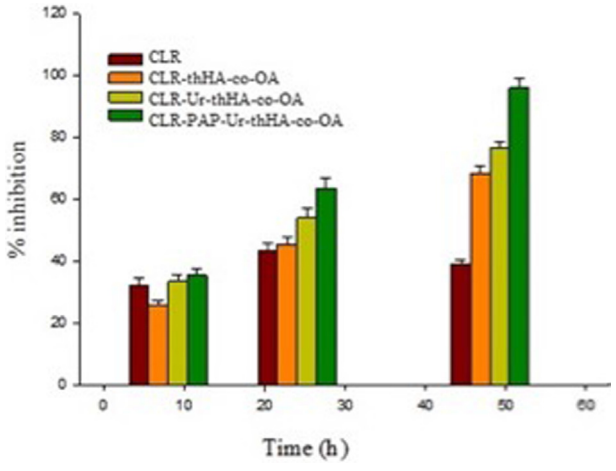

Fig. 10. Growth inhibition of *H. pylori* induced by free CLR suspension, CLR-thHA-co-OA, CLR-Ur-thHA-co-OA and CLR-PAP-Ur-thHA-co-OA nanomicelles at 48 h of incubation. Mean values are presented as ± SD (n = 3).

Table 4
H. pylori clearance effect of various drug-loaded nanoformulations.

Colony counts	Dose (mg/Kg)		
	5	7.5	10
Physiological saline	131	122	119
Clarithromycin powder	104	86	55
CLR-thHA-co-OA	65	47	31
CLR-Ur-thHA-co-OA	42	28	12
CLR-PAP-Ur-thHA-co-OA	18	10	4

70%, 80% and almost 100% growth inhibition after 48 h, respectively. The observed improved *in vitro* efficacy for nanomicelles as compared to free drug suspension agrees with the role played by the polymeric composition of nanomicelles, the prolonged release profile of drug, and a high eradication rate.

3.9. In vivo H. Pylori clearance study

An in vivo *H. pylori* clearance study was conducted in order to investigate the in vivo efficacy of various drug-loaded nanomicelles in comparison to pure free clarithromycin powder. Drug was administered in 3 different doses. The results shown in Table 4 showed a significant increase in *H. pylori* clearance for CLR-thHA-co-OA, CLR-Ur-thHA-co-OA and CLR-PAP-Ur-thHA-co-OA nanomicelles in comparison to free clarithromycin. CLR-PAP-Ur-thHA-co-OA nanocarrier showed the highest reduction (ca. 30-fold) in bacterial burden in comparison to the other nanoformulations and control at a dose of 10 mg/kg probably thanks to a greater bioavailability of the nanocarrier system [34].

4. Conclusions

CLR-PAP-Ur-thHA-co-OA nanomicelles were successfully prepared with improved mucoadhesive and mucus penetrating properties. CLR-PAP-Ur-thHA-co-OA nanomicelles, owing to the presence of papain, were able to cleave mucoglycoproteins. A prolonged release drug pattern and stability at acidic pH was exhibited by the selected nanoformulations. CLR-PAP-Ur-thHA-co-OA nanomicelles showed an improved antibacterial effect against *H. pylori* as compared to free administered clarithromycin. Overall, the newly developed CLR-PAP-Ur-thHA-co-OA nanomicelles have the potential to be an efficient nanocarrier for *H. pylori* infection treatment thanks to their enhanced mucopenetration and mucoadhesion properties, as well as their improved stability and extended drug release.

CRediT authorship contribution statement

Aimen Qaiser: Investigation, Data curation, Methodology, Writing – review & editing. **Maria Hassan Kiani:** Conceptualization, Methodology, Writing – review & editing. **Rashida Parveen:** . **Muhammad Sarfaraz:** . **Gul Shahnaz:** Funding acquisition, Validation, Visualization, Writing – review & editing. **Abbas Rahdar:** Methodology, Writing – review & editing. **Pablo Taboada:** Validation, Visualization, Writing – review & editing.

Declaration of Competing Interest

The authors declare that they have no known competing financial interests or personal relationships that could have appeared to influence the work reported in this paper.

Acknowledgements

The authors acknowledge financial support provided by Quaid-i-Azam University for this work. We acknowledge Riphah Institute of Pharmacy and Microbiology Department of Quaid-i-Azam University, Islamabad for their lab services. P.T also thanks Agencia Estatal de Investigación (AEI) by project PID2019-109517RB-I00. ERDF funds are also acknowledged.

References

[1] A. Lanas, F.K. Chan, Peptic ulcer disease, Lancet 390 (10094) (2017) 613–624, https://doi.org/10.1016/S0140-6736(16)32404-7.
[2] C.S. Goodwin, Histology and ultrastructure of helicobacter pylori infections: gastritis, duodenitis, and peptic ulceration, and their relevance asprecancerous conditions, in: Helicobacter pylori Biology and Clinical Practice, CRC Press, 2018, pp. 37–62.
[3] S.A. Azer, H. Akhondi, Gastritis, in StatPearls [Internet], 2019. StatPearls Publishing. <https://www.ncbi.nlm.nih.gov/books/NBK544250/>.
[4] P. Floch, F. Mégraud, P. Lehours, Helicobacter pylori strains and gastric MALT lymphoma, Toxins 9 (4) (2017) 132, https://doi.org/10.3390/toxins9040132.
[5] K.O. Alfarouk, A.H.H. Bashir, A.N. Aljarbou, A.M. Ramadan, A.K. Muddathir, S.T. S. AlHoufie, A. Hifny, G.O. Elhassan, M.E. Ibrahim, S.S. Alqahtani, S.D. AlSharari, C.T. Supuran, C. Rauch, R.A. Cardone, S.J. Reshkin, S. Fais, S. Harguindey, The possible role of helicobacter pylori in gastric cancer and its management, Front. Oncol. 9 (2019), https://doi.org/10.3389/fonc.2019.00075.
[6] C.M. den Hoed, E.J. Kuipers, Helicobacter pylori infection, in: Hunter's Tropical Medicine and Emerging Infectious Diseases, Elsevier, 2020, pp. 476–480.
[7] P. Sipponen, M. Sturala, C.S. Goodwin, Histology and ultrastructure of helicobacter pylori infections: gastritis, duodenitis, and peptic ulceration, and their relevance asprecancerous conditions, Helicobacter Pylori Biol. Clin. Pract. (2018) 37–62, https://doi.org/10.1201/9781351073165.
[8] R.M. Zagari, S. Rabitti, L.H. Eusebi, F. Bazzoli, Treatment of Helicobacter pylori infection: a clinical practice update, Eur. J. Clin. 48 (1) (2018) e12857, https://doi.org/10.1111/eci.12857.
[9] E.A. Marcus, G. Sachs, D.R. Scott, Eradication of Helicobacter pylori infection, Curr. Gastroenterol. Rep. 18 (7) (2016) 33, https://doi.org/10.1007/s11894-016-0509-x.
[10] D. Lopes, C. Nunes, M.C.L. Martins, B. Sarmento, S. Reis, Eradication of Helicobacter pylori: past, present and future, J. Control Release 189 (2014) 169–186, https://doi.org/10.1016/j.jconrel.2014.06.020.
[11] M. Zhang, High antibiotic resistance rate: a difficult issue for Helicobacter pylori eradication treatment, World J. Gastroenterol. 21 (48) (2015) 13432, https://doi.org/10.3748/wjg.v21.i48.13432.
[12] S. Arora, G. Bisen, R.D. Budhiraja, Mucoadhesive and muco-penetrating delivery systems for eradication of Helicobacter pylori, Asian J. Pharm. 6 (2012) 18–30, https://doi.org/10.4103/0973-8398.100127.
[13] J. Ding, R. He, G. Zhou, C. Tang, C. Yin, Multilayered mucoadhesive hydrogel films based on thiolated hyaluronic acid and polyvinylalcohol for insulin delivery, Acta Biomater. 8 (10) (2012) 3643–3651, https://doi.org/10.1016/j.actbio.2012.06.027.
[14] B. Luppi, F. Bigucci, L. Mercolini, A. Musenga, M. Sorrenti, L. Catenacci, V. Zecchi, Novel mucoadhesive nasal inserts based on chitosan/hyaluronate polyelectrolyte complexes for peptide and protein delivery, J. Pharm. Pharmacol. 61 (2) (2010) 151–157.
[15] X. Zheng Shu, Y. Liu, F.S. Palumbo, Y.i. Luo, G.D. Prestwich, In situ crosslinkable hyaluronan hydrogels for tissue engineering, Biomaterials 25 (7-8) (2004) 1339–1348, https://doi.org/10.1016/j.biomaterials.2003.08.014.
[16] K.N. Garg et al., Mucosal delivery of vaccines: role of mucoadhesive/biodegradable polymers, Recent Pat Drug Deliv. Formul. 4 (2) (2010) 114–128, https://doi.org/10.2174/187221110791185015.
[17] A.-M. Vasi, M.I. Popa, M. Butnaru, G. Dodi, L. Verestiuc, Chemical functionalization of hyaluronic acid for drug delivery applications, Mater. Sci. Eng. C 38 (2014) 177–185, https://doi.org/10.1016/j.msec.2014.01.052.
[18] R.K. Mishra, S.K. Tiwari, S. Mohapatra, S. Thomas, Efficient nanocarriers for drug-delivery systems: types and fabrication, in: Nanocarriers for Drug Delivery, Elsevier, 2019, pp. 1–41, https://doi.org/10.1016/B978-0-12-814033-8.00001-1.
[19] S.W. Jung, S.W. Lee, The antibacterial effect of fatty acids on Helicobacter pylori infection, Korean J. Intern. Med. 31 (1) (2016) 30, https://doi.org/10.3904/kjim.2016.31.1.30.
[20] Z.-W. Jing, Y.-Y. Jia, N. Wan, M. Luo, M.-L. Huan, T.-B. Kang, S.-Y. Zhou, B.-L. Zhang, Design and evaluation of novel pH-sensitive ureido-conjugated chitosan/TPP nanoparticles targeted to Helicobacter pylori, Biomaterials 84 (2016) 276–285, https://doi.org/10.1016/j.biomaterials.2016.01.045.
[21] A. Batool, R. Arshad, S. Razzaq, K. Nousheen, M.H. Kiani, G. Shahnaz, Formulation and evaluation of hyaluronic acid-based mucoadhesive self nanoemulsifying drug delivery system (SNEDDS) of tamoxifen for targeting breast cancer, Int. J. Biol. Macromol. 152 (2020) 503–515, https://doi.org/10.1016/j.ijbiomac.2020.02.275.
[22] A. Mahmood, M. Lanthaler, F. Laffleur, C.W. Huck, A. Bernkop-Schnürch, Thiolated chitosan micelles: highly mucoadhesive drug carriers, Carbohydr. Polym. 167 (2017) 250–258, https://doi.org/10.1016/j.carbpol.2017.03.019.
[23] Y.-S. Jian et al., hyaluronic acid–nimesulide conjugates as anticancer drugs against cD44-overexpressing hT-29 colorectal cancer in vitro and in vivo, Int. J. Nanomed. 12 (2017) 2315, https://doi.org/10.2147/IJN.S120847.
[24] X. Wang, J. Iqbal, D. Rahmat, A. Bernkop-Schnürch, Preactivated thiomers: permeation enhancing properties, Int. J. Pharm. 438 (1–2) (2012) 217–224, https://doi.org/10.1016/j.ijpharm.2012.08.045.
[25] S. Dünnhaupt, J. Barthelmes, J. Hombach, D. Sakloetsakun, V. Arkhipova, A. Bernkop-Schnürch, Distribution of thiolated mucoadhesive nanoparticles on intestinal mucosa, Int. J. Pharm. 408 (1–2) (2011) 191–199, https://doi.org/10.1016/j.ijpharm.2011.01.060.
[26] J. Iqbal, G. Shahnaz, G. Perera, F. Hintzen, F. Sarti, A. Bernkop-Schnürch, Thiolated chitosan: development and in vivo evaluation of an oral delivery system for leuprolide, Eur. J. Pharm. Biopharm. 80 (1) (2012) 95–102, https://doi.org/10.1016/j.ejpb.2011.09.010.
[27] M. Qindeel, N. Ahmed, K.U. Shah, N. Ullah, Asim.ur.Rehman, New, environment friendly approach for synthesis of amphiphilic PCL–PEG–PCL triblock copolymer: an efficient carrier for fabrication of nanomicelles, J. Polym. Environ. 28 (4) (2020) 1237–1251, https://doi.org/10.1007/s10924-020-01683-1.
[28] G. Shahnaz, G. Perera, D. Sakloetsakun, D. Rahmat, A. Bernkop-Schnürch, Synthesis, characterization, mucoadhesion and biocompatibility of thiolated carboxymethyl dextran–cysteine conjugate, J. Control Release 144 (1) (2010) 32–38, https://doi.org/10.1016/j.jconrel.2010.01.033.
[29] Y. Cong, J. Geng, H. Wang, J. Su, M. Arif, Q. Dong, Z. Chi, C. Liu, Ureido-modified carboxymethyl chitosan-graft-stearic acid polymeric nano-micelles as a targeted delivering carrier of clarithromycin for Helicobacter pylori: preparation and in vitro evaluation, Int. J. Biol. Macromol. 129 (2019) 686–692, https://doi.org/10.1016/j.ijbiomac.2019.01.227.
[30] C. Leichner, C. Menzel, F. Laffleur, A. Bernkop-Schnürch, Development and in vitro characterization of a papain loaded mucolytic self-emulsifying drug delivery system (SEDDS), Int. J. Pharm. 530 (1-2) (2017) 346–353, https://doi.org/10.1016/j.ijpharm.2017.08.059.
[31] A.M. Newton, S. Kaur, Solid lipid nanoparticles for skin and drug delivery: Methods of preparation and characterization techniques and applications, in: Nanoarchitectonics in Biomedicine, Elsevier, 2019, pp. 295–334.
[32] S. Köllner, S. Dünnhaupt, C. Waldner, S. Hauptstein, I. Pereira de Sousa, A. Bernkop-Schnürch, Mucus permeating thiomer nanoparticles, Eur. J. Pharm. Biopharm. 97 (2015) 265–272, https://doi.org/10.1016/j.ejpb.2015.01.004.
[33] C. Müller, K. Leithner, S. Hauptstein, F. Hintzen, W. Salvenmoser, A. Bernkop-Schnürch, Preparation and characterization of mucus-penetrating papain/poly (acrylic acid) nanoparticles for oral drug delivery applications, J. Nanopart Res. 15 (1) (2013), https://doi.org/10.1007/s11051-012-1353-z.
[34] S. Thamphiwatana, W. Gao, M. Obonyo, L. Zhang, In vivo treatment of Helicobacter pylori infection with liposomal linolenic acid reduces colonization and ameliorates inflammation, Proc. Natl. Acad. Sci. 111 (49) (2014) 17600–17605, https://doi.org/10.1073/pnas.1418230111.
[35] M. Narkar, P. Sher, A. Pawar, Stomach-specific controlled release gellan beads of acid-soluble drug prepared by ionotropic gelation method, AAPS PharmSciTech 11 (1) (2010) 267–277, https://doi.org/10.1208/s12249-010-9384-1.
[36] J.K. Patel, J.R. Chavda, Formulation and evaluation of stomach-specific amoxicillin-loaded carbopol-934P mucoadhesive microspheres for anti-Helicobacter pylori therapy, J. Microencapsul. 26 (4) (2009) 365–376, https://doi.org/10.1080/02652040802373012.
[37] R.A. Cone, Barrier properties of mucus, Adv. Drug Deliv. Rev. 61 (2) (2009) 75–85, https://doi.org/10.1016/j.addr.2008.09.008.
[38] S. Arora et al., Amoxicillin loaded chitosan–alginate polyelectrolyte complex nanoparticles as mucopenetrating delivery system for H. pylori, Sci. Pharm. 79 (3) (2011) 673–694, https://doi.org/10.3797/scipharm.1011-05.
[39] S. Arora, G. Bisen, R. Budhiraja, Mucoadhesive and muco-penetrating delivery systems for eradication of Helicobacter pylori, Asian J. Pharmaceut. (AJP): Free Full Text Articles Asian J. Pharm. 6 (1) (2014), https://doi.org/10.22377/AJP.V6I1.69.
[40] W. Tsung-Chung, Mixture of hyaluronic acid for treating and preventing peptic ulcer and duodenal ulcer, Google Patents, 2014.
[41] S. Khulusi, H.A. Ahmed, P. Patel, M.A. Mendall, T.C. Northfield, The effects of unsaturated fatty acids on Helicobacter pylori in vitro, J. Med. Microbiol. 42 (4) (1995) 276–282, https://doi.org/10.1099/00222615-42-4-276.
[42] S.S. Kesharwani, R. Dachineni, G.J. Bhat, H. Tummala, Hydrophobically modified inulin-based micelles: transport mechanisms and drug delivery applications for breast cancer, J. Drug Deliv. Sci. Technol. 54 (2019) 101254, https://doi.org/10.1016/j.jddst.2019.101254.
[43] Z.-W. Jing, M. Luo, Y.-Y. Jia, C. Li, S.-Y. Zhou, Q.-B. Mei, B.-L. Zhang, Anti-Helicobacter pylori effectiveness and targeted delivery performance of amoxicillin-UCCs-2/TPP nanoparticles based on ureido-modified chitosan derivative, Int. J. Biol. Macromol. 115 (2018) 367–374, https://doi.org/10.1016/j.ijbiomac.2018.04.070.
[44] M.A. Gauthier, H.-A. Klok, Polymer–protein conjugates: an enzymatic activity perspective, Polym. Chem. 1 (9) (2010) 1352–1373, https://doi.org/10.1039/C0PY90001J.
[45] J. Carneiro, P.M. Döll-Boscardin, B.C. Fiorin, J.M. Nadal, P.V. Farago, J.P.d. Paula, Development and characterization of hyaluronic acid-lysine nanoparticles with potential as innovative dermal filling, Braz. J. Pharm. Sci. 52 (4) (2016) 645–651.
[46] M. Tavakkoli Yaraki, M. Tayebi, M. Ahmadieh, M. Tahriri, D. Vashaee, L. Tayebi, Synthesis and optical properties of cysteamine-capped ZnS quantum dots for aflatoxin quantification, J. Alloys Compd. 690 (2017) 749–758, https://doi.org/10.1016/j.jallcom.2016.08.158.

[47] L. Zhang, R. He, H.-C. Gu, Oleic acid coating on the monodisperse magnetite nanoparticles, Appl. Surf. Sci. 253 (5) (2006) 2611–2617, https://doi.org/10.1016/j.apsusc.2006.05.023.
[48] M. Manivannan, S. Rajendran, Investigation of inhibitive action of urea–Zn 2+ system in the corrosion control of carbon steel in sea water, Int. J. Eng. Sci. Technol 3 (2011) 8048–8060.
[49] C.S. Brazel, N.A. Peppas, Modeling of drug release from swellable polymers, Eur. J. Pharm. Biopharm. 49 (1) (2000) 47–58, https://doi.org/10.1016/s0939-6411(99)00058-2.
[50] I. Shahzadi, A. Fürst, Z.B. Akkus-Dagdeviren, S. Arshad, M. Kurpiers, B. Matuszczak, A. Bernkop-Schnürch, Less reactive thiol ligands: key towards highly mucoadhesive drug delivery systems, Polymers 12 (6) (2020) 1259, https://doi.org/10.3390/polym12061259.
[51] S. De Robertis, M.C. Bonferoni, L. Elviri, G. Sandri, C. Caramella, R. Bettini, Advances in oral controlled drug delivery: the role of drug–polymer and interpolymer non-covalent interactions, Exp. Opin. Drug Deliv. 12 (3) (2015) 441–453, https://doi.org/10.1517/17425247.2015.966685.
[52] A. Bernkop-Schnürch, S. Steininger, Synthesis and characterisation of mucoadhesive thiolated polymers, Int. J. Pharm. 194 (2) (2000) 239–247, https://doi.org/10.1016/s0378-5173(99)00387-7.
[53] Y. Feng, J. Lin, L. Niu, Y. Wang, Z. Cheng, X. Sun, M. Li, High molecular weight silk fibroin prepared by papain degumming, Polymers 12 (9) (2020) 2105, https://doi.org/10.3390/polym12092105.
[54] H. Liu et al., Unimolecular micelles: synthesis and characterization of amphiphilic polymer systems, J. Polym. Sci. A Polym. Chem. 37 (6) (1999) 703–711, https://doi.org/10.1002/(SICI)1099-0518(19990315)37:6<703::AID-POLA5>3.0.CO;2-O.
[55] P.R. Sharma, A.J. Varma, Thermal stability of cellulose and their nanoparticles: effect of incremental increases in carboxyl and aldehyde groups, Carbohydr. Polym. 114 (2014) 339–343, https://doi.org/10.1016/j.carbpol.2014.08.032.
[56] M. Sharma, N. Gupta, S. Gupta, Implications of designing clarithromycin loaded solid lipid nanoparticles on their pharmacokinetics, antibacterial activity and safety, RSC Adv. 6 (80) (2016) 76621–76631, https://doi.org/10.1039/C6RA12841F.
[57] A.J. Shnoudeh, I. Hamad, R.W. Abdo, L. Qadumii, A.Y. Jaber, H.S. Surchi, S.Z. Alkelany, in: Biomaterials and Bionanotechnology, Elsevier, 2019, pp. 527–612, https://doi.org/10.1016/B978-0-12-814427-5.00015-9.
[58] E. Joseph, G. Singhvi, Multifunctional nanocrystals for cancer therapy: a potential nanocarrier, Nanomater. Drug Deliv Therapy (2019) 91–116, https://doi.org/10.1016/B978-0-12-816505-8.00007-2.
[59] A. Doostmohammadi, A. Monshi, R. Salehi, M.H. Fathi, Z. Golniya, A.U. Daniels, Bioactive glass nanoparticles with negative zeta potential, Ceram. Int. 37 (7) (2011) 2311–2316, https://doi.org/10.1016/j.ceramint.2011.03.026.
[60] Diao, Y.-Y., et al., Doxorubicin-loaded PEG-PCL copolymer micelles enhance cytotoxicity and intracellular accumulation of doxorubicin in adriamycin-resistant tumor cells. Int. J. Nanomed. 6 (2011) 1955. doi:10.2147/IJN.S23099.
[61] F. Madsen, K. Eberth, J.D. Smart, A rheological examination of the mucoadhesive/mucus interaction: the effect of mucoadhesive type and concentration, J Control Release 50 (1–3) (1998) 167–178, https://doi.org/10.1016/s0168-3659(97)00138-7.
[62] S. Dünnhaupt, J. Barthelmes, D. Rahmat, K. Leithner, C.C. Thurner, H. Friedl, A. Bernkop-Schnürch, S-protected thiolated chitosan for oral delivery of hydrophilic macromolecules: evaluation of permeation enhancing and efflux pump inhibitory properties, Mol. Pharm. 9 (5) (2012) 1331–1341, https://doi.org/10.1021/mp200598j.
[63] S.K. Lai, Y.-Y. Wang, J. Hanes, Mucus-penetrating nanoparticles for drug and gene delivery to mucosal tissues, Adv. Drug Deliv. Rev. 61 (2) (2009) 158–171, https://doi.org/10.1016/j.addr.2008.11.002.